459 **8. Supplementary information**

460 *8.1. Model morphology*

461   The morphology parameters needed to construct the cell, lorica, and collar surface, are given in
462 Table S1. The parameters serve as inputs for equation (2).

Table S1. Morphology parameters for the lorica and cell outline. The parameters are used in equation (2).

|	R_0 [µm]	α_1 [rad]	α_2 [rad]	α_3 [rad]
Cell	2.8 ± 0.3	-0.24	0.10	-0.10
Lorica	8.1 ± 0.4	0.15	0.05	0.00
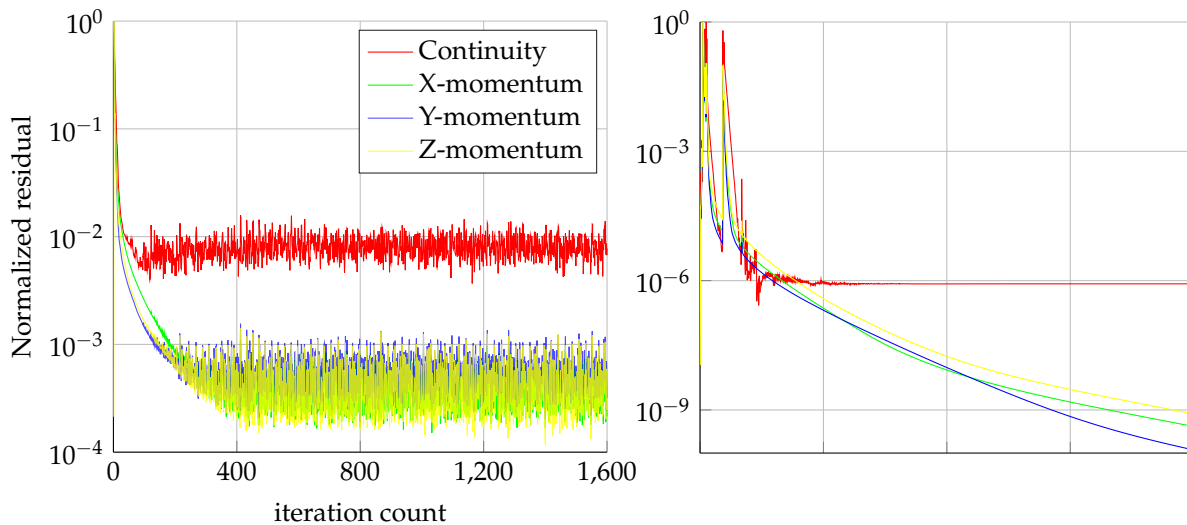
Figure S1. The top plot displays the residuals for one time step (1600 iterations) when applying a pressure boundary condition to the domain. The bottom plot displays the residuals for one time step when applying a zero inlet velocity boundary condition to the domain. All data series in both plots have been normalized based on their maximum value.

463 *8.2. Residuals*

464   We conclude in Section 2.1.2 that a computational domain with a radius of 30 µm produces results
465 of sufficient accuracy. Hence, applying an inlet velocity of 0 µm/s to the outer domain boundary
466 suffices. The drawback of this boundary condition is that it creates visible flow recirculation and
467 for this reason, the flow around the model organism does not bear resemblance to what would be
468 observed in reality. However, the recirculation does not affect the flow characteristics studied in this
469 paper. Alternatively, a pressure outlet boundary condition can be applied to the outer domain surface
470 instead of the zero velocity inlet condition. The pressure boundary condition ensures the same level of
471 accuracy in results and mimics the real life behavior of the flow around the model organism much
472 better. The drawback of the pressure boundary condition is that it does not satisfy continuity to the
473 same extend as the velocity boundary condition cf. Figure S1. Conclusively, we choose to accept the
474 heightened residuals and apply a pressure boundary condition to the outer domain surface.

475 *8.3. Mesh*

476   The mesh is primarily discretized by polyhedral cells as they are advantageous for complex model
477 geometries like choanoflagellates. Prism layers are added to the prey and the microvilli surfaces, in
478 order to capture the steep solution gradients near the no-slip boundaries (Figure S3). The mesh is
479 refined by decreasing the surface size of the microvilli and prey surface simultaneously. For the loricate
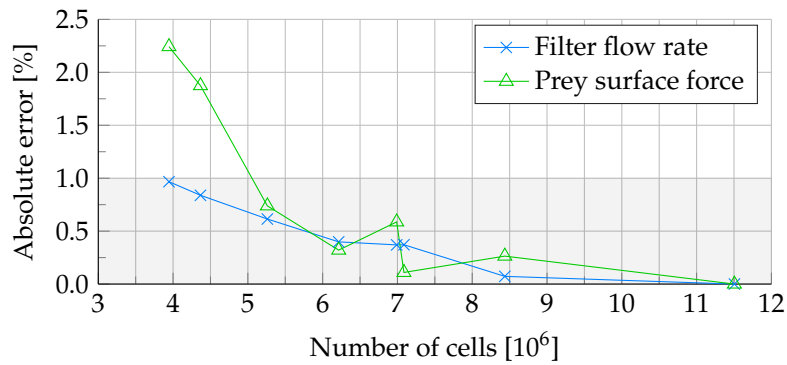
Figure S2. Percentage error in results when comparing coarser meshes to the *exact solution*, represented by a mesh of $\sim$ 11 million cells. Here, the time-averaged flow rate through the filter and the time-averaged total prey force were monitored for one beat cycle and used for comparison.

480 *D. grandis* we refine the mesh up until 11 million cells. The finest mesh we denote the *exact solution*.
481 The coarser meshes are compared to the exact solution, for which we obtain $< 1\%$ variation in results
482 for meshes with 5 million cells or more (Figure S2).

483 *8.4. Convergence of dynamic results*

In each iteration we monitor the force and the torque on the prey in all directions in space, totaling six degrees of freedom. The forces are converted into linear velocities, $\boldsymbol{U}$, using Stokes law (equation (10)) and the torques are converted into angular velocities $\boldsymbol{\Omega}$ using[1]:

$$\boldsymbol{L} = 8\pi\mu r^3 \boldsymbol{\Omega}. \tag{S1}$$

484 These resultant linear and angular velocities can then readily be compared to the linear and angular
485 velocities we assign to the prey movement in each iteration, using equation (12). We stop iterating
486 when each directional component of the linear and angular velocities calculated from the torques and
487 forces, are below 0.1% of each of the directional components of the prey's linear and angular velocity.
488 Here, we have employed zero initial velocity and rotation in the first time step only. In all of the
489 subsequent time steps the terminal velocity and rotation of the preceding time step serves as the initial
490 guess. The terminal linear and angular velocities are found to be independent of the initial guess and
491 thus the convergence level of 0.1% is satisfied in *all* time steps.

---

1   Leach, J.; Mushfique, H.; Keen, S.; Di Leonardo, R.; Ruocco, G.; Cooper, J. M.; Padgett, M. Comparison of Faxen's correction for a microsphere translating or rotating near a surface. *Phys. Rev. E* **2009**, *79*, 026301.
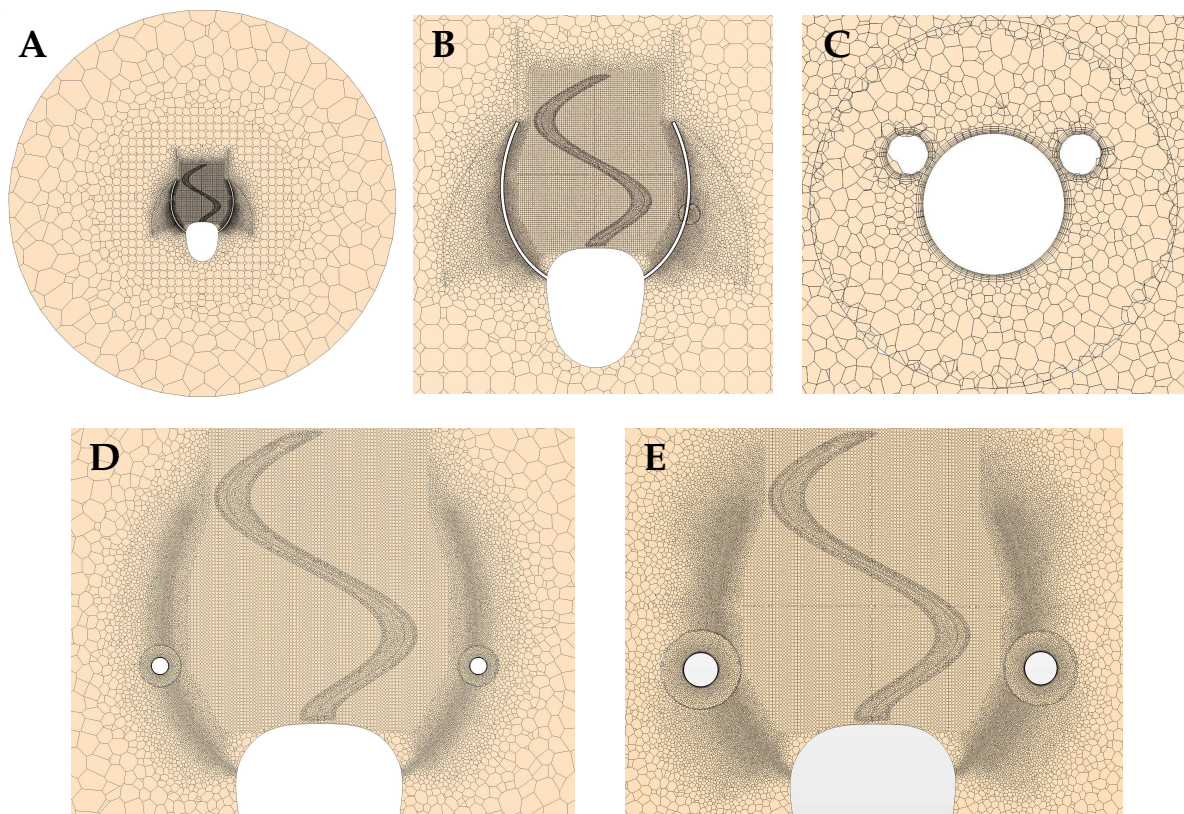
Figure S3. Illustrations of the mesh used in both the static and dynamic simulations. (A) The entire computational domain. (B) The loricate *D. grandis* pictured in a plane that intersect two microvilli. (C) Closeup of the overset mesh around a medium sized prey (large circle), placed in between two microvilli (small circles) viewed in a horizontal plane tangent to the collar. (D) The non-loricate *D. grandis* shown with medium sized prey. (E) The non-loricate *D. grandis* shown with large prey, where the region of refined cells near the collar has been extended such that it covers the size of the enlarged prey overset mesh.